

Water-molecule dissociation by impact of He⁺ ions

P. M. Y. Garcia and G. M. Sigaud

Departamento de Física, Pontifícia Universidade Católica do Rio de Janeiro, Caixa Postal 38071, Rio de Janeiro, Rio de Janeiro 22452-970, Brazil

H. Luna

Centro Brasileiro de Pesquisas Físicas, R. Dr. Xavier Sigaud 150, Rio de Janeiro, Rio de Janeiro 22290-180, Brazil

A. C. F. Santos and E. C. Montenegro

Instituto de Física, Universidade Federal do Rio de Janeiro, Caixa Postal 68528, Rio de Janeiro, Rio de Janeiro 21945-970, Brazil

M. B. Shah

Department of Physics and Astronomy, The Queen's University of Belfast, Northern Ireland, United Kingdom

(Received 27 February 2008; published 15 May 2008)

Absolute cross sections for the ionization and fragmentation of water vapor molecules during collisions with 0.5 to 2.0 MeV He⁺ ions, resulting from pure ionization, projectile electron loss, and projectile electron capture processes, have been measured. The masses and charge states of the recoil ions have been detected by time-of-flight spectroscopy in coincidence with the emergent charge states of the projectile. The projectile energy range includes the Bragg peak, where the energy deposition rate by the projectile reaches its maximum. It was observed that the fragmentation patterns depend not only on the projectile characteristics, such as velocity and effective charge state, but also on the particular collision channel involved.

DOI: [10.1103/PhysRevA.77.052708](https://doi.org/10.1103/PhysRevA.77.052708)

PACS number(s): 34.50.Fa, 52.20.Hv

I. INTRODUCTION

The study of the interaction of energetic ions, electrons and photons with the water molecule is important to many branches of Science, from the understanding of the fundamental processes of molecular fragmentation to applications in astrophysics, biology, and medicine. Of particular interest are the collision processes which lead to molecular dissociation, because highly reactive products, such as OH⁺, O⁺, and H⁺, can affect the local environment by means of chemical reactions [1]. One of the most important applications of such collisions leading to the radiolysis of the water molecule is related to the potential damage that these products can cause to water-filled biological living cells [2,3]. For instance, apoptosis can either be enhanced or inhibited by the inflammatory oxidant H₂O₂, which can be produced by recombinations of the above-cited fragmentation products [4].

In recent years there has been an increasing interest in the use of a cancer therapy called radioimmunotherapy (RIT), where a radionuclide is delivered to a tumor tissue either directly or associated with an antibody specifically tailored to bind preferentially to antigens overexpressed on tumor cells, thereby permitting to deliver large amounts of energy specifically to these cells, leaving the surrounding normal tissues relatively unharmed [5]. Through a combination of antibodies and radionuclides with properties which are compatible with the intended therapeutic application, RIT is particularly useful in the treatment of refractory cancer cases, such as small solid tumors and micrometastases [6,7]. Initially conceived to be used employing β -particle emitters, in the last few years it has been extended to α -particle-emitting nuclides, due to their much higher linear energy transfer and much shorter path length in comparison with β particles, resulting in a higher absorbed dose and a larger number of

ionization events in a range corresponding to the cell diameter [6]. For this reason, it has been speculated that only a few α particles would be necessary to cause cell death [6]. However, in some cases, such as cells which have large nuclei or high radiosensitivities, recent microdosimetric simulations have indicated that the average number of hits to the cell nucleus required to eradicate a tumor cell population with a high probability can be as high as 100 [8]. With these doses, the radiolysis of the surrounding water starts to become important and, due to the chemistry with the resulting water radicals, the probability of causing damage to healthy tissues around a tumor also becomes of concern.

The choice of the α -emitter radionuclide depends on several factors, including availability and costs of production. The most promising candidates up to now have been ²¹¹At, ²²⁵Ac, its daughter product ²¹³Bi, and ²¹²Bi [5–7,9]. The energies of the α -particles emitted by these nuclides are in the range between 5.0 and 8.5 MeV.

Radiolysis of water is also of considerable interest in astrophysics. The interaction between multiply charged ions of the solar wind and neutral atoms and molecules, either in the interstellar medium [10,11] or in cometary coma [12], results in x-ray emission, which is directly correlated with the wind parameters such as composition, mass, and velocity [13–15]. The solar wind also interacts with the atmospheres and surfaces of planets and satellites of the Solar system. Space probes to Mars, Jupiter, and Saturn have recently sent data which indicates the presence of water in these planets. A more detailed understanding of the fragmentation of the water molecule induced by collisions with energetic charged particles is, thus, of great importance to help modeling of the formation of planetary atmospheres; it could, for instance, explain the high concentration of oxygen in Europa's atmosphere.

However, the literature concerning the experimental study of water molecular dissociation in the gas phase by energetic heavy ions is still rather scarce. The largest amount of data refers to proton impact, since the pioneering work of Toburen *et al.* [16] for total electron capture and electron loss cross sections, followed by studies of doubly differential ionization cross section [17–19] and measurements of cross sections of positive ion production, electron production, and electron capture [20]. Only recently, data on partial absolute dissociation cross sections by proton impact, differential in the possible collision channels, became available [21–24].

For heavier ions the situation is even worse. There are few data for water fragmentation by C and O ions in the region around the Bragg peak [1,25,26]. For He ions as projectiles, the only available data are those from Rudd *et al.* of absolute cross sections for ionization, electron capture and electron loss for He⁺ in the energy range between 5 and 450 keV [27], and low-energy measurements by Seredyuk *et al.* (0.1–48 keV He²⁺, electron capture and transfer-ionization channels) [28], Sobocinski *et al.* (1–5 keV He²⁺, absolute differential cross sections, differential in the emission angle of the fragments) [29], and Alvarado *et al.* (kinetic energy releases of 2–20 keV He⁺ and He²⁺ ions) [30]. Although important for water radiolysis and astrophysical studies, these data do not cover some important aspects of the ionization and fragmentation of the water molecule by He ions, since they lie below the maximum of the Bragg peak, where the energy deposition rate in water by the He projectile is largest.

In the present paper we have measured absolute cross sections for the collision processes which can be summarized by



where $n=0, 1$, or 2 represent the electron capture, pure ionization or electron loss processes, respectively, while $[\text{H}_2\text{O}]^{m+}$ denote the water target product ions, which include not only the ion H₂O⁺, but also, the fragment ions H⁺, OH⁺, O⁺, and, in some instances, O²⁺. The cross sections were

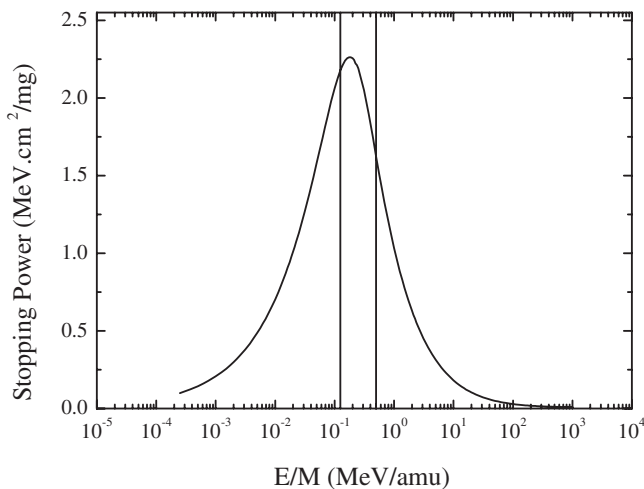


FIG. 1. Stopping power of He⁺ ions in water [31]. The vertical lines represent the energy region of the data covered in the present work.

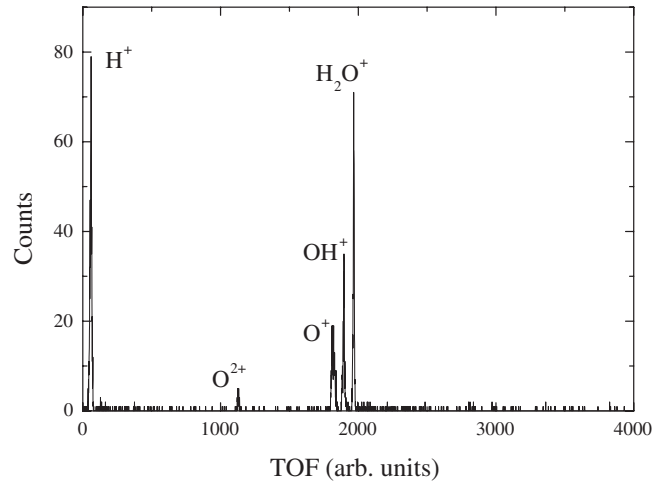


FIG. 2. Time-of-flight spectrum for one-electron-capture collisions by incident 0.5 MeV He⁺ projectiles on water vapor.

obtained by means of coincident measurements, for He⁺ projectiles with energies ranging from 0.5 to 2.0 MeV. This energy range includes the Bragg peak for He⁺ in water, as shown in Fig. 1.

As mentioned above, in the case of RIT, the emitted α -particles have energies which lie a little above the energy range of the present measurements with He⁺ projectiles. However, the α -particles will reach the target cells or their environments not only with energies within the range of the data presented here, but also, with probabilities of presenting a charge state of +1 that vary from 4% at 2.0 MeV up to 58% at 0.5 MeV [32].

II. EXPERIMENT

Since detailed descriptions of the experimental setup used for the measurements performed in this work have been given previously [24,33–35], only its most important features will be presented here. Briefly, monoenergetic He⁺ beams, with energies ranging from 0.5 to 2.0 MeV, are delivered by the 4MV Van de Graaff accelerator of the Catholic University of Rio de Janeiro. The selection of charge, mass and energy of the beam is made by a 90° magnet followed by a switching magnet before the entrance of the beam line. The beam is collimated and separated from its spurious components by a third magnet placed just before the collision chamber.

TABLE I. Absolute fragment and nonfragment production cross sections (in Mb) of H₂O by He⁺ impact as a function of the projectile energy E : pure ionization channel.

E (MeV)	H ₂ O ⁺	OH ⁺	H ⁺	O ⁺
0.5	282 ± 35	101 ± 15	140 ± 19	42.5 ± 5.4
0.75	90 ± 13	31.8 ± 6.0	124 ± 15	36.2 ± 6.6
1.0	164 ± 19	52.5 ± 6.2	59.9 ± 7.0	20.3 ± 2.6
1.5	162 ± 18	44.1 ± 5.2	46.9 ± 5.5	12.7 ± 1.7
2.0	117 ± 13	36.2 ± 4.3	35.5 ± 4.2	6.3 ± 0.9

TABLE II. Absolute fragment and nonfragment production cross sections (in Mb) of H₂O by He⁺ impact as a function of the projectile energy, E : electron loss channel.

E (MeV)	H ₂ O ⁺	OH ⁺	H ⁺	O ⁺	O ²⁺
0.5	20.8 ± 2.6	13.5 ± 1.8	39.2 ± 4.7	20.1 ± 2.6	3.1 ± 0.6
0.75	12.5 ± 1.6	9.9 ± 1.3	40.0 ± 5.2	14.1 ± 1.2	0.86 ± 0.14
1.0	23.7 ± 3.0	12.0 ± 1.6	26.6 ± 3.8	13.0 ± 2.2	
1.5	28.0 ± 3.4	10.9 ± 1.5	23.2 ± 2.8	8.2 ± 1.1	
2.0	28.8 ± 3.5	12.1 ± 1.6	21.0 ± 2.6	7.5 ± 1.1	

After crossing the collision chamber where the gas cell is placed, the emergent beam is charge-analyzed by a fourth magnet, which separates the three possible charge states and directs them onto a position sensitive microchannelplate (MCP) detector placed at the end of the beam line 4 m downstream. The target is formed by an effusive water vapor setup. A manifold connecting a needle valve to a Pyrex bottle containing 10 ml of deionized water is primarily pumped by an external rough pump. The pressure inside the bottle decreases until the water turns into ice; at this stage, all the gases (mainly, N₂ and O₂) have been pumped out of the bottle. The pump is then turned off and the iced water is warmed up. In order to guarantee that one has a pure H₂O target, the process is repeated to drive out any remaining dissolved gas. The ice is then allowed to sublimate into the gas cell and the flux is controlled by the connecting needle valve. The pressure inside the gas cell is measured by an absolute capacitive manometer (MKS-Baratron). Determination of the gas pressure for water vapor is more difficult than for standard molecular gases. Working with H₂O requires longer times for the capacitance diaphragm to reach the equilibrium (order of a few minutes as opposed to some seconds for noble gases, for instance) and significant drifts of the zero reading can occur. This has been overcome by performing sets of shorter measuring runs and checking the zero reading of the gauge at each run. The pressures inside the target cell during the measurements were kept between 0.7 to 1 mTorr. Without the target, the pressure is smaller than 10⁻⁶ Torr.

The charged target products, H⁺, OH⁺, H₂O⁺, O⁺, and O²⁺, resulting from the interaction with the incident He⁺ beam are collected by a transverse electric field. The use of a strong electric field (960 V/cm) assures a maximum collecting efficiency for all target products [24]. The slow ions traverse the electrodes, enter into a field free region, and finally are collected by a second MCP detector. The target products, including the dissociative and nondissociative component, are separated and analyzed by a standard time-of-flight coincidence technique. In Fig. 2, we present the

time-of-flight spectrum for the electron capture channel by 0.5 MeV He⁺ projectiles from the water molecule.

The recoil ion detection efficiencies are obtained using the same procedure described by Santos *et al.* [33,34]. For a detailed description of the coincidence procedure and the gas cell setup see also the above-cited references.

III. RESULTS AND DISCUSSION

Our results for the absolute cross sections for the pure ionization, electron loss and electron capture processes, as represented in Eq. (1), are shown in Tables I–III, respectively. An inspection of these tables reveals that pure ionization is the dominant channel for all target ion product channels over the whole energy range of this work. This is an indication that, within the present velocity region, large impact parameter collisions dominate the ionization processes, meaning that the projectile charge state as seen by the target is essentially 1. Thus, it seems reasonable to compare the present He⁺ results for the pure ionization channel with the corresponding proton data. This is done in Fig. 3, where we compare our results with the proton impact data of Ref. [24] covering the 15 to 100 keV and 500 to 3500 keV energy ranges, for the total positive ion production as well as for the individual target ion channels. It can be seen that, apparently, the present He⁺ data follow the general trends of the high-velocity proton data of Ref. [24] for all the collision products. However, the agreement with the low-velocity proton data is not so good. Except for the H⁺ production, which seems to couple quite well with the He⁺ ones, the other reaction products exhibit different behaviors: the O⁺ production by He⁺ exceeds that by protons by a factor of 2 at a velocity around 2.0 a.u., while although the lower-velocity He⁺ cross sections for H₂O⁺ and OH⁺ match the proton ones, they present a dip around 2.5 a.u.

In order to further examine this peculiar behavior, the present He⁺ pure ionization data for the H₂O⁺ production channel (full circles) are compared with similar proton data

TABLE III. Absolute fragment and nonfragment production cross sections (in Mb) of H₂O by He⁺ impact as a function of the projectile energy, E : electron capture channel.

E (MeV)	H ₂ O ⁺	OH ⁺	H ⁺	O ⁺	O ²⁺
0.5	5.4 ± 0.6	3.2 ± 0.4	8.1 ± 1.0	3.4 ± 0.4	0.43 ± 0.08
0.75	11.0 ± 1.3	6.0 ± 0.7	11.0 ± 2.0	4.9 ± 0.6	0.86 ± 0.14
1.0	2.7 ± 0.5	1.4 ± 0.4	2.9 ± 0.6	1.3 ± 0.3	

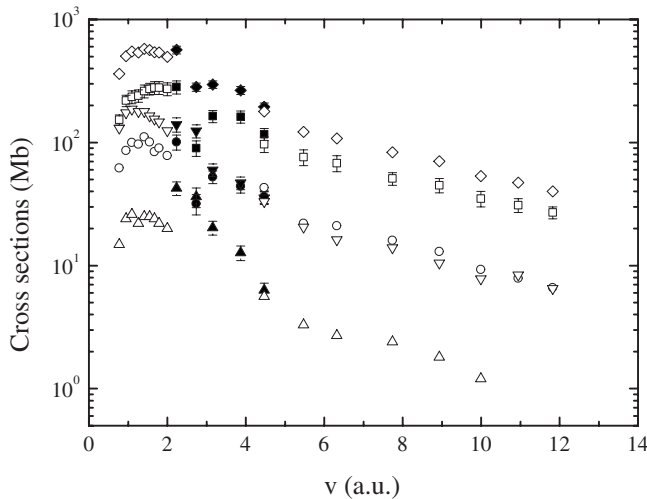


FIG. 3. Absolute single ionization and fragment production cross sections (in Mb) of H_2O by He^+ (full symbols, this work) and proton (open symbols, Ref. [24]) impact as a function of the projectile velocity: pure ionization channel. Squares, H_2O^+ ; circles, OH^+ ; inverted triangles, H^+ ; up triangles, O^+ ; and diamonds, total positive ion production.

from Refs. [21–24] (open symbols) and for C^{3+} projectile from Ref. [1] (full squares) in Fig. 4. An important feature that arises from the analysis of this graph is that the values of the absolute cross sections are the same for the three projectiles. This independence of the cross sections with the projectile charge state was already observed by Luna and Montenegro for protons and C^{3+} projectiles [1]. However, there is a remarkable difference here, since the proton data vary smoothly with the projectile velocity, while the dip around 2.5 a.u. mentioned above for He^+ also occurs for C^{3+} , at the same velocity and with the same numerical values. In Fig. 5, on the other hand, we compare the present set of He^+ data with the results from Rudd *et al.* for the same projectile [27],

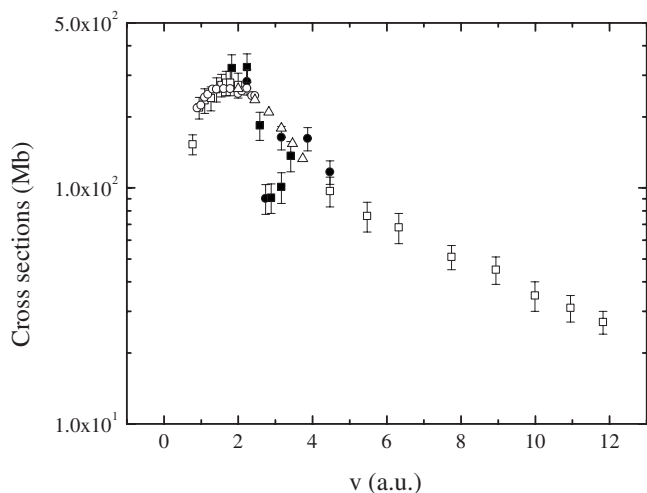


FIG. 4. Absolute single ionization cross sections (in Mb) of H_2O by He^+ , C^{3+} and proton impact as a function of the projectile velocity for the pure ionization channel. Projectiles: He^+ , full circles, this work; C^{3+} , full squares, Ref. [1]; protons, open squares, Ref. [24], open triangles, Ref. [21], open circles, Refs. [22,23].

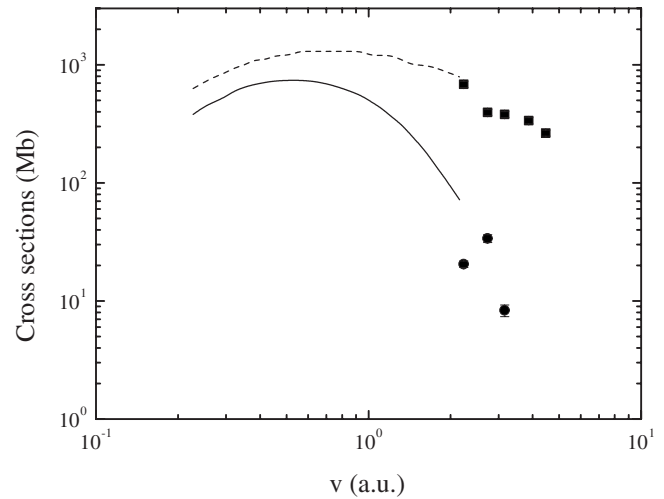


FIG. 5. Absolute cross sections (in Mb) for total positive ion production and electron capture of H_2O by He^+ impact as a function of the projectile velocity. Total positive ion production: full squares, this work; dashed line, Ref. [27]. Electron capture: full circles, this work; full line, Ref. [27].

which are the only data set in the literature which almost overlap with ours, for the total positive ion production (σ_+ , dashed line and full squares) and for the capture channel only (full line and full circles). It can be observed that the dip around the velocity of 2.5 a.u. still appears in σ_+ and corresponds to an enhancement in the capture cross section. However, this velocity corresponds to the maximum of the Bragg peak, as can be seen from Fig. 1, for He^+ , and from Ref. [26], for example, for C^+ projectiles in water. The fact that these projectiles have more complex structures than protons opens, in the velocity range considered here, other collision channels besides the pure ionization one. These other channels, essentially electron loss and electron capture, have larger contributions from smaller impact parameters than pure ionization. This decreases the cross sections for the latter process around the maximum of the energy deposition on the target. This is, thus, an indication that the effective charge of the projectile plays an important role in the process of energy transfer to the active electrons of the molecule.

The different dynamical regimes for the ionization and fragmentation of the water vapor molecule can be better analyzed by means of a ternary plot which presents the normalized fractions of the different reaction products. As pointed out by Luna and Montenegro [1], this type of graph is very useful for the comparison between data from different projectiles and collision processes. So, the present He^+ data is compared with experimental data obtained with other projectiles in the ternary plot of Fig. 6. The axes represent the fractions of the H_2O^+ (bottom), OH^+ (right), and the sum of all positive O ions (left), relative to the total ion production, for different projectiles and collision processes. The projectiles are He^+ (full squares, this work), protons (circles, Ref. [24]), C^{3+} (triangles, Ref. [1]), O^{5+} (diamonds, Ref. [1]), electrons (inverted triangles, Ref. [36]), and stars (photons, Ref. [37]). In this figure, the collision processes considered are pure ionization, electron loss and electron capture; however, they are not explicitly shown in this figure to avoid confusion.

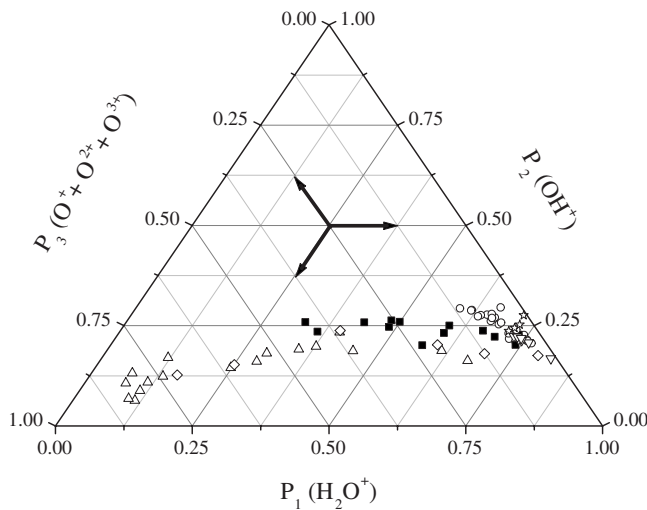


FIG. 6. Ternary plot of the fractions of the H₂O⁺ (bottom), OH⁺ (right), and Oⁿ⁺ (left) ions produced in collisions of H₂O with several projectiles and for the pure ionization, electron loss and electron capture channels. Projectiles: He⁺, full squares, this work; protons, circles, Ref. [24]; C³⁺, triangles, Ref. [1]; O⁵⁺, diamonds, Ref. [1]; electrons, inverted triangles, Ref. [36]; and stars, photons, Ref. [37]. The specific collision channels are not explicitly shown in the graph. The three arrows in the middle upper side of the plot indicate how a particular data point is connected with each of the three axes [1].

A remarkable feature of this kind of plot—which was first observed by Luna and Montenegro [1]—is that all the data, independently of the projectile and process, coalesce along a line, with the larger energy-transfer data concentrated on the left side (larger Oⁿ⁺ production—explosive fragmentation regime) and the lighter ion data on the right side (larger H₂O⁺ production—dipolar fragmentation regime). Our He⁺ data lie, as expected, in the intermediate region, following the general trend of all other data.

However, in Fig. 6 there are information neither on the specific collision process which is taking place, nor on the collision velocity of each point in the graph. Thus, in Figs. 7–9 ternary plots for the different collision processes which contribute to molecular fragmentation, namely, pure ionization, electron loss, and electron capture, respectively, for He⁺ (full lines) and C³⁺ (dashed lines) projectiles are presented. The arrows indicate the direction of increasing projectile velocity, which varies from 2.2 to 4.5 a.u. for He⁺ and from 1.8 to 3.4 a.u. for C³⁺.

There are two points which are common to all these three plots and should be stressed. First, the data for the electron loss and electron capture channels lie more to the left of the graphs than the pure ionization one, which means that the former two processes are more effective than the latter for the explosive fragmentation of the water molecule. This feature is expected since the electron loss and capture are processes which can reach smaller impact parameters than the pure ionization, thus being more able to ionize the inner-shell electrons of the water molecule. This inner-shell ionization may lead to the postcollisional ionization of the molecule, as is well known to occur in small-impact-parameter processes in ion-atom collisions [38]. In this sense, the transition from

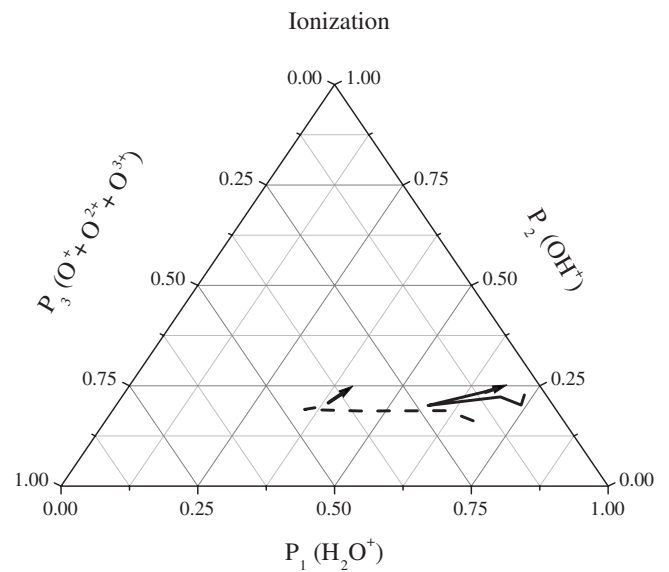


FIG. 7. Ternary plot of the fractions of the H₂O⁺ (bottom), OH⁺ (right), and O⁺ (left) ions produced in collisions of H₂O with He⁺ (full line, this work) and C³⁺ (dashed line, Ref. [1]) for the pure ionization channel. The arrows indicate the direction of increasing collision velocity.

dipolar to explosive dissociation can be interpreted as corresponding to an enhancement of the multiple ionization process. Second, and perhaps more important, is the fact that all collision channels present a similar behavior with the projectile velocity for both projectiles: as the velocity increases the fragmentation first tends to follow an explosive pattern, presenting, however, a turning point, after which the fragmentation tends back to the dipolar pattern. This turning point, for both projectiles and all collision channels, lies very close to the maximum of the Bragg peak. The only difference between the two projectiles lies on the fact that the C³⁺ data are always more to the left than the He⁺ ones, which simply reinforces the expected feature that C³⁺ is more effective to produce explosive fragmentation than He⁺.

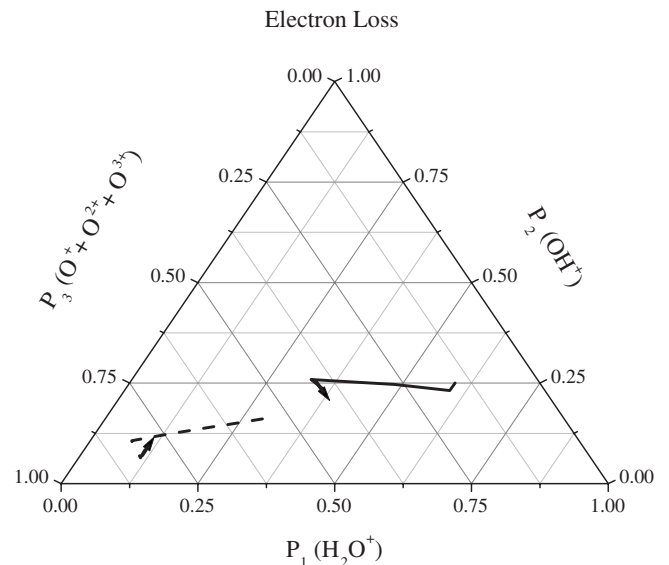


FIG. 8. The same as in Fig. 7 for the electron loss channel.

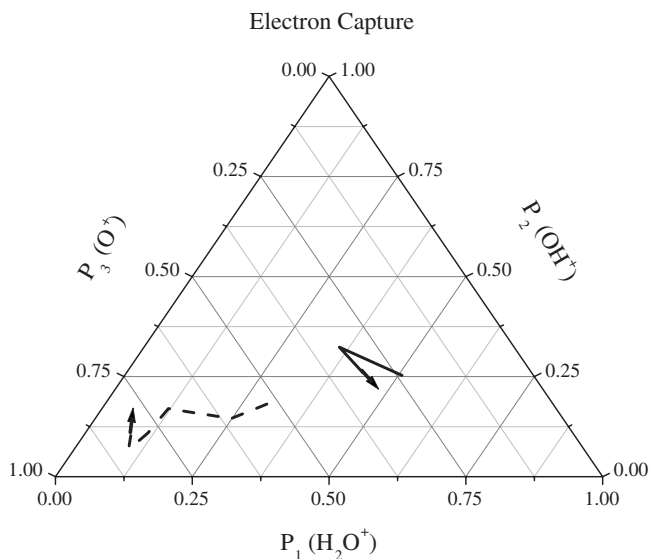


FIG. 9. The same as in Fig. 7 for the electron capture channel.

IV. CONCLUSIONS

We have measured absolute cross sections for the ionization and fragmentation of water vapor molecules in collisions with He^+ ions, differential in the pure target ionization, electron loss, and electron capture processes, in a velocity range that includes the maximum of the Bragg peak. It was observed that the fragmentation patterns depend not only on the projectile characteristics, such as velocity and effective charge state, but also on the particular collision mechanism. In the case of the pure ionization channel, for instance, the cross sections for the production of the molecular ion H_2O^+ by He^+ have the same values as those by C^{3+} projectiles,

being strongly inhibited around the Bragg peak in comparison with the corresponding proton data. This is due to the opening of other collision channels, such as electron loss and capture, in addition to the pure ionization for more complex projectiles in the velocity range of the present measurements.

The comparison of the present measurements for the normalized fractions of the different collision products with results for several other projectiles, including photons and electrons as well as heavy ions, by means of ternary plots, shows that the He^+ data lie in the intermediate region between the dipolar and explosive fragmentation regimes. When compared to C^{3+} data, separated by reaction channel and considering the velocity dependence of the fractions, the results for He^+ show similar behaviors for all collision channels as the collision velocity increases, all presenting a turning point in the tendency from dipolar to explosive fragmentation at a velocity corresponding to the maximum of the Bragg peak.

The present data are useful to provide further information about the transition from the dipolar to the explosive regimes of the fragmentation of the water molecule, stressing the importance not only of the projectile velocity and structure as, for instance, its charge state, but also, the reaction channels taking place. They may be important, for instance, to help the implementation of new therapies, such as radioimmunotherapy with α -particle emitters, where detailed reference data for microdosimetric analyses and simulations are crucial to the interpretation of the clinical results and in the design of treatment strategies to achieve a favorable therapeutic outcome.

ACKNOWLEDGMENTS

This work was supported in part by the Brazilian agencies CNPq and FAPERJ.

-
- [1] H. Luna and E. C. Montenegro, *Phys. Rev. Lett.* **94**, 043201 (2005).
- [2] E. J. Hall, *Radiobiology for the Radiologist*, 5th ed. (Lippincott, Williams, & Wilkins, Philadelphia, PA, 2000).
- [3] A. Brahme, *Int. J. Radiat. Oncol. Biol. Phys.* **58**, 603 (2004).
- [4] H. Chang, W. Oehrl, P. Elsner, and J. J. Thiele, *Free Radic. Res.* **37**, 655 (2003).
- [5] T. G. Stinchcomb and J. C. Roeske, *Med. Phys.* **19**, 1385 (1992).
- [6] O. Couturier, S. Supiot, M. Degraef-Mougin, A. Faivre-Chauvet, T. Carlier, J.-F. Chatal, F. Davodeau, and M. Cherel, *Eur. J. Nucl. Med. Mol. Imaging* **32**, 601 (2005).
- [7] M. R. Zalutsky, D. A. Reardon, O. R. Pozzi, G. Vaidyanathan, and D. D. Bigner, *Nucl. Med. Biol.* **34**, 779 (2007).
- [8] J. C. Roeske and T. G. Stinchcomb, *Phys. Med. Biol.* **51**, 179 (2006).
- [9] S. Sofou, B. J. Kappel, J. S. Jaggi, M. R. McDevitt, D. A. Scheinberg, and G. Sgouros, *Bioconjug. Chem.* **18**, 2061 (2007).
- [10] T. E. Cravens, *Geophys. Res. Lett.* **24**, 105 (1997).
- [11] V. Kharchenko and A. Dalgarno, *J. Geophys. Res.* **105**, 18351 (2000).
- [12] T. E. Cravens, *Science* **296**, 1042 (2002).
- [13] V. Kharchenko and A. Dalgarno, *Astrophys. J.* **554**, L99 (2001).
- [14] V. Kharchenko, M. Rigazio, A. Dalgarno, and V. A. Krasnopolsky, *Astrophys. J.* **585**, L73 (2003).
- [15] D. Bodewits, Z. Juhász, R. Hoekstra, and A. G. G. M. Tielens, *Astrophys. J.* **606**, L81 (2004).
- [16] L. H. Toburen, M. Y. Nakai, and R. A. Langley, *Phys. Rev.* **171**, 114 (1968).
- [17] L. H. Toburen and W. E. Wilson, *J. Chem. Phys.* **66**, 5202 (1977).
- [18] L. H. Toburen, W. E. Wilson, and R. J. Popowich, *Radiat. Res.* **82**, 27 (1980).
- [19] M. A. Bolorizadeh and M. E. Rudd, *Phys. Rev. A* **33**, 888 (1986).
- [20] M. E. Rudd, T. V. Goffe, R. D. DuBois, and L. H. Toburen, *Phys. Rev. A* **31**, 492 (1985).
- [21] U. Werner, K. Beckord, J. Becker, and H. O. Lutz, *Phys. Rev.*

- Lett. **74**, 1962 (1995).
- [22] F. Gobet, B. Farizon, M. Farizon, M. J. Gaillard, M. Carré, M. Lezius, P. Scheier, and T. D. Mark, Phys. Rev. Lett. **86**, 3751 (2001).
- [23] F. Gobet, S. Eden, B. Coupier, J. Tabet, B. Farizon, M. Farizon, M. J. Gaillard, M. Carré, S. Ouaskit, T. D. Mark, and P. Scheier, Phys. Rev. A **70**, 062716 (2004).
- [24] H. Luna, A. L. F. de Barros, J. A. Wyer, S. W. J. Scully, J. Lecointre, P. M. Y. Garcia, G. M. Sigaud, A. C. F. Santos, V. Senthil, M. B. Shah, C. J. Latimer, and E. C. Montenegro, Phys. Rev. A **75**, 042711 (2007).
- [25] H. Luna, P. M. Y. Garcia, G. M. Sigaud, M. B. Shah, and E. C. Montenegro, in *Photonic, Electronic and Atomic Collisions*, edited by P. D. Fainstein, M. A. P. Lima, J. E. Miraglia, E. C. Montenegro, and R. D. Rivarola (World Scientific, Singapore, 2006), pp. 439–449.
- [26] E. C. Montenegro, M. B. Shah, H. Luna, S. W. J. Scully, A. L. F. de Barros, J. A. Wyer, and J. Lecointre, Phys. Rev. Lett. **99**, 213201 (2007).
- [27] M. E. Rudd, A. Itoh, and T. V. Goffe, Phys. Rev. A **32**, 2499 (1985).
- [28] B. Seredyuk *et al.*, Phys. Rev. A **71**, 022705 (2005).
- [29] P. Sobocinski, Z. D. Pešić, R. Hellhammer, N. Stolterfoht, B. Sulik, S. Legendre, and J.-Y. Chesnel, J. Phys. B **38**, 2495 (2005).
- [30] F. Alvarado, R. Hoekstra, and T. Schlathöler, J. Phys. B **38**, 4085 (2005).
- [31] H. Paul and A. Schinner, At. Data Nucl. Data Tables **85**, 377 (2003). (MSTAR version 3 available from <http://www.exphys.unilinz.ac.at/Stopping/>.)
- [32] P. L. Grande and G. Schiwietz, Nucl. Instrum. Methods Phys. Res. B **195**, 55 (2002). (CasP, version 3.1 available from <http://www.hmi.de/people/schiwietz/casp.html>.)
- [33] A. C. F. Santos, W. S. Melo, M. M. Sant’Anna, G. M. Sigaud, and E. C. Montenegro, Phys. Rev. A **63**, 062717 (2001).
- [34] A. C. F. Santos, W. S. Melo, M. M. Sant’Anna, G. M. Sigaud, and E. C. Montenegro, Rev. Sci. Instrum. **73**, 2369 (2002).
- [35] E. Cavalcanti, G. M. Sigaud, E. C. Montenegro, M. M. Sant’Anna, and H. Schmidt-Böcking, J. Phys. B **35**, 3937 (2002).
- [36] M. V. V. Rao, I. Iga, and S. K. Srivastava, J. Geophys. Res. **100**, 26421 (1995).
- [37] K. H. Tan, C. E. Brion, Ph. E. Van der Leeuw, and M. J. Van der Wiel, Chem. Phys. **29**, 299 (1978).
- [38] T. Kirchner, A. C. F. Santos, H. Luna, M. M. Sant’Anna, W. S. Melo, G. M. Sigaud, and E. C. Montenegro, Phys. Rev. A **72**, 012707 (2005).